Line of polarization attraction in highly birefringent optical fibers

M. Guasoni, E. Assémat, P. Morin, A. Picozzi, J. Fatome, S. Pitois, H. R. Jauslin, G. Millot, and D. Sugny*

Laboratoire Interdisciplinaire Carnot de Bourgogne (ICB), UMR 6303 CNRS-Université de Bourgogne, Dijon, France
**Corresponding author: dominique.sugny@u-bourgogne.fr*

Received November 1, 2013; revised January 19, 2014; accepted January 19, 2014;
posted January 21, 2014 (Doc. ID 200367); published February 26, 2014

We investigate the phenomenon of polarization attraction in a highly birefringent fiber. This polarization process originates from the nonlinear interaction of two counter-propagating beams. We show that all polarization states of the forward (signal) beam are attracted toward a specific line of polarization states on the surface of the Poincaré sphere, whose characteristics are determined by the polarization state of the injected backward (pump) beam. This phenomenon of polarization attraction takes place without any loss of energy for the signal beam. The stability of different stationary solutions is also discussed through intensive numerical simulations. On the basis of mathematical techniques recently developed for the study of Hamiltonian singularities, we provide a detailed description of this spontaneous polarization process. In several particular cases of interest, the equation of the line of polarization attraction on the Poincaré sphere can be obtained in explicit analytical form.

OCIS codes: (190.4370) Nonlinear optics, fibers; (060.4370) Nonlinear optics, fibers; (190.0190) Nonlinear optics.
http://dx.doi.org/10.1364/JOSAB.31.000572

1. INTRODUCTION

Since the pioneering work by Heebner *et al.* in 2000, who proposed a "universal polarizer" performing polarization of unpolarized light with 100% efficiency [1], the possibility of achieving spontaneous polarization of unpolarized light in a nonlinear Kerr medium has been the subject of growing interest, with important applications in optical fiber telecommunications. Contrarily to conventional polarizers, which are known to waste 50% of unpolarized light, Heebner *et al.* (2000) proposed a "universal polarizer" performing polarization of unpolarized light with 100% efficiency [1]. This phenomenon has been called "polarization attraction," in the sense that all input polarization configurations are transformed into a well-defined polarization state. This effect of spontaneous polarization has been subsequently demonstrated in the framework of a counter-propagating configuration of the four-wave interaction in optical fiber systems [2].

This repolarization effect was unexpected because the nonlinear Kerr effect was known to lead to depolarization processes, as has been discussed in different works [3–5]. Following the observation [2], phenomena of polarization attraction, or pulling have been studied in optical fiber systems in several configurations, e.g., involving the Raman effect [6–14], or Brillouin backscattering [15]. We note that, in this respect, beyond its natural importance in potential applications in optical fiber telecommunications, Raman-based polarization pulling processes have been shown to exhibit unexpected phenomena of stochastic resonance and dynamic localization, which have been reported in [9] in relation to fundamental problems of activated escape from metastable states in periodically forced systems [16].

On the other hand, polarization attraction through the conservative backward four-wave interaction has been the subject of growing interest, from both the theoretical [17–24] and experimental [2,25–28] points of view. It is important to underline that the phenomenon of polarization attraction has been shown to exhibit different properties, which depend on the experimental configuration [29,30], and on the type of optical fiber used, e.g., isotropic fibers [2,18,19,25], highly birefringent (HB) spun fibers [22,31], as well as randomly birefringent fibers used in optical telecommunications [21,22,26]. Along this line, it has been shown that polarization attraction can even occur in the absence of any injected backward beam—the signal beam interacts with its own counter-propagating replica, which is produced by means of a back-reflection Bragg-mirror at the fiber output [29,30]. From a different perspective, the possibility of achieving polarization attraction has been also discussed in the copropagating configuration in the case of a large group-velocity difference between the two beams [32,33].

Most of the theoretical works developed to describe this phenomenon of polarization attraction have been focused on intensive numerical simulations of the spatio-temporal dynamics and on the derivation of the equations governing the evolutions of the counter-propagating beams in different types of optical fiber systems. On the other hand, a theoretical description of the properties of polarization attraction has been obtained using mathematical techniques recently developed for the study of Hamiltonian singularities [34,35]. In particular, this geometrical approach revealed the essential role played in the process of polarization attraction by the peculiar topological properties of singular tori. We refer the reader to Ref. [36] for a recent review devoted to the applicability of singular reduction theory to the problem of polarization attraction.

The aim of this paper is to extend these works by showing that the phenomenon of polarization attraction also occurs in a HB optical fiber. We show that HB optical fibers exhibit a

polarization attraction whose properties differ from those encountered in the conventional phenomenon. In the usual attraction process, the states of polarization (SOP) of the forward signal beam converge to a single (or several) SOP(s), whereas in HB fibers all signal SOPs are attracted toward a specific line of polarization states on the surface of the Poincaré sphere. This process can be described through the geometrical analysis of the stationary singular states of the system. In certain cases, this allows us to derive an explicit analytical expression of the line of polarization attraction on the surface of the Poincaré sphere. Our theoretical results are confirmed by extensive numerical simulations of the counter-propagating equations. This phenomenon of attraction on a specific line of polarization states is similar to that described in optical spun fibers [22], although the properties of this process were not analyzed in detail in previous works. Our analysis reveals a novel feature: the spreading of signal SOPs on the line of polarization attraction decreases in a substantial way as the pump power or the fiber length are increased. We will see that this property entails the possibility of achieving novel forms of polarization processes. Moreover, the phenomenon of polarization attraction on a specific line on the Poincaré sphere has not yet been observed experimentally, presumably because of the inherent specificity of spun optical fibers. By showing the existence of lines of polarization attraction in the framework of conventional HB fiber systems, we can expect the experimental observation of this remarkable phenomenon in a near future.

The paper is organized as follows. In Section 2, we introduce the partial differential system governing the dynamics of the two counter-propagating waves in HB optical fibers. These equations are formulated in terms of the Stokes parameters, which prove appropriate for the theoretical study. Section 3 is devoted to the geometrical study of the stationary system. In particular, we give the positions and the properties of the different singular states of the system. In Section 4, in relation to the theoretical study, we present a complete numerical analysis of the process of polarization attraction in a HB fiber for different configurations. Some conclusions and discussions are presented in Section 5.

2. MODEL SYSTEM

We consider the counter-propagating interaction of two beams in a conventional HB optical fiber. The equations governing the evolution of the amplitudes of the field envelopes can be written in the following form:

$$
\begin{aligned}
(\partial_t + v_g\partial_z)E_x &= i\gamma\left(|E_x|^2 + \frac{2}{3}|E_y|^2 + 2|\overline{E}_x|^2 + \frac{2}{3}|\overline{E}_y|^2\right)E_x + \frac{2i\gamma}{3}E_y\overline{E_yE_x}^*\\
(\partial_t + v_g\partial_z)E_y &= i\gamma\left(|E_y|^2 + \frac{2}{3}|E_x|^2 + 2|\overline{E}_y|^2 + \frac{2}{3}|\overline{E}_x|^2\right)E_y + \frac{2i\gamma}{3}E_x\overline{E_xE_y}^*\\
(\partial_t - v_g\partial_z)\overline{E}_x &= i\gamma\left(|\overline{E}_x|^2 + \frac{2}{3}|\overline{E}_y|^2 + 2|E_x|^2 + \frac{2}{3}|E_y|^2\right)\overline{E}_x + \frac{2i\gamma}{3}\overline{E}_yE_yE_x^*\\
(\partial_t - v_g\partial_z)\overline{E}_y &= i\gamma\left(|\overline{E}_y|^2 + \frac{2}{3}|\overline{E}_x|^2 + 2|E_y|^2 + \frac{2}{3}|E_x|^2\right)\overline{E}_y + \frac{2i\gamma}{3}\overline{E}_xE_xE_y^*,
\end{aligned}
\tag{1}
$$

where the optical fields (E_x, E_y, E_z) and $(\overline{E}_x, \overline{E}_y, \overline{E}_z)$ correspond, respectively, to the forward and backward beams. The variable z denotes the spatial coordinate along the fiber, γ is the nonlinear Kerr coefficient, and v_g the group-velocity of the waves in the optical fiber. Note that we can neglect the group-velocity difference between the copropagating orthogonal polarization components E_x and E_y (as well as $\overline{E}_x$ and $\overline{E}_y$). The introduction of the basis of circular polarization states:

$$
u = \frac{E_x + iE_y}{\sqrt{12}}, \qquad v = \frac{E_x - iE_y}{\sqrt{12}},
$$
$$
\overline{u} = \frac{\overline{E}_x + i\overline{E}_y}{\sqrt{12}}, \qquad \overline{v} = \frac{\overline{E}_x - i\overline{E}_y}{\sqrt{12}},
$$

allows us to write the governing equations into the following form

$$
\begin{aligned}
(\partial_t + v_g\partial_z)u &= i\gamma(5|u|^2 + 6|v|^2 + 6|\overline{u}|^2 + 10|\overline{v}|^2)u\\
&\quad + i\gamma(6\overline{v}^*\overline{u} + 2\overline{u}^*\overline{v} + vu^*)v\\
(\partial_t + v_g\partial_z)v &= i\gamma(5|v|^2 + 6|u|^2 + 6|\overline{v}|^2 + 10|\overline{u}|^2)v\\
&\quad + i\gamma(6\overline{u}^*\overline{v} + 2\overline{v}^*\overline{u} + uv^*)u\\
(\partial_t - v_g\partial_z)\overline{u} &= i\gamma(5|\overline{u}|^2 + 6|\overline{v}|^2 + 6|u|^2 + 10|v|^2)\overline{u}\\
&\quad + i\gamma(6v^*u + 2u^*v + \overline{vu}^*)\overline{v}\\
(\partial_t - v_g\partial_z)\overline{v} &= i\gamma(5|\overline{v}|^2 + 6|\overline{u}|^2 + 6|v|^2 + 10|u|^2)\overline{v}\\
&\quad + i\gamma(6u^*v + 2v^*u + \overline{uv}^*)\overline{u}.
\end{aligned}
\tag{2}
$$

The Stokes vectors $\vec{S} = (S_1, S_2, S_3)$ and $\vec{J} = (J_1, J_2, J_3)$, which describe, respectively, the polarization states of the forward and backward beams on the Poincaré sphere, are defined by

$$
\begin{cases} S_1 = i(u^*v - uv^*) \\ S_2 = u^*v + uv^* \\ S_3 = |u|^2 - |v|^2 \end{cases}, \qquad \begin{cases} J_1 = i(\overline{u}^*\overline{v} - \overline{uv}^*) \\ J_2 = \overline{u}^*\overline{v} + \overline{uv}^* \\ J_3 = |\overline{u}|^2 - |\overline{v}|^2 \end{cases}.
$$

The radii of the forward and backward Poincaré spheres, S_0 and J_0, refer to the signal and pump powers, $S_0 = (E_x^2 + E_y^2)/6$ and $J_0 = (\overline{E}_x^2 + \overline{E}_y^2)/6$, respectively. Plugging the Stokes vectors into Eq. (2) gives

$$
\begin{cases} \frac{\partial\vec{S}}{\partial t} + \frac{\partial\vec{S}}{\partial z} = \vec{S}\times(\mathcal{I}_s\vec{S}) + \vec{S}\times(\mathcal{I}_i\vec{J}) \\ \frac{\partial\vec{J}}{\partial t} - \frac{\partial\vec{J}}{\partial z} = \vec{J}\times(\mathcal{I}_s\vec{J}) + \vec{J}\times(\mathcal{I}_i\vec{S}) \end{cases},
\tag{3}
$$

where the matrices $\mathcal{I}_s = \mathrm{Diag}(0, 2, 0)$ and $\mathcal{I}_i = \mathrm{Diag}(4, 8, -4)$ are diagonal. The symbol "×" denotes, here, the vector

product. Note that, for convenience, the equations described as Eq. (3) have been normalized with respect to the nonlinear time $\tau_0 = 1/(\gamma J_0)$ and length $\Lambda = v_g \tau_0$ while the Stokes vectors have been normalized with respect to J_0. The variables can be recovered in real units through the transformation, $t \to t\tau_0, z \to z\Lambda, (\vec{S}, \vec{J}) \to (\vec{S}, \vec{J})J_0$. Accordingly, the dimensionless fiber length, say L, is measured in units of the nonlinear length Λ—a variation of L by a factor α can be obtained in a real experiment by varying either the fiber length or the pump power by the same factor [see Ref. [18] for more details regarding the scale invariance of Eq. (3)].

3. GEOMETRICAL ANALYSIS OF THE STATIONARY SYSTEM

As for the conventional polarization attraction, the numerical simulations of Eq. (3) reveal that, in many cases, the spatio-temporal dynamics exhibit a relaxation process toward a stationary state. This aspect will be discussed through different examples in Section 4. Hence, our approach is based on the study of the singularities of the stationary Hamiltonian trajectories. In particular, it was shown in [17,19,22,36] that the stationary states selected by the spatio-temporal dynamics lie on the surface of a singular torus, which can be viewed as a two-dimensional extension of the concept of separatrix, well-known for systems with one degree of freedom. The singular torus thus plays the role of an attractor for the wave system [17]. We refer the reader to Ref. [36] for a detailed presentation of the singular reduction theory employed to determine the topological properties of the singular tori. This geometrical approach is only briefly explained here.

The starting point is the analysis of the properties of the stationary solutions of the spatio-temporal Eq. (3). Dropping the time derivatives, it is straightforward to show that this system has a Hamiltonian structure defined by

$$H = -4S_1J_1 - 8S_2J_2 + 4S_3J_3 - S_2^2 - J_2^2, \tag{4}$$

where the coordinate z plays, here, the role of time. This two-degree of freedom system, with Hamiltonian H, is Liouville integrable because it admits another constant of motion $K = S_2 + J_2$. Accordingly, the stationary system has the same number of constants of motion as degrees of freedom and it is called integrable [37]. As a consequence, the corresponding phase-space is organized into tori characterized by different values of H and K. A global overview of the Hamiltonian dynamics is provided by the so-called energy–momentum diagram, which can be defined as the ensemble of all possible values of H and K for some given fixed powers of the counter-propagating beams.

The energy–momentum diagram is plotted in Fig. 1 for identical powers of the beams $S_0 = J_0 = 1$, and has been constructed using singular reduction theory, which can be viewed, in simple terms, as a change of variables that exploits the constant of the motion K to reduce the dimensionality of the problem [36]. This approach provides the positions of the singular states in the (H, K)-plane, and also determines the topological structure of the corresponding singular tori. Here, the singular states are represented by solid lines in Fig. 1. In particular, we observe a line of bitori, which will play a central role in the phenomenon of polarization attraction. As discussed in [36], a bitorus is a particular example of

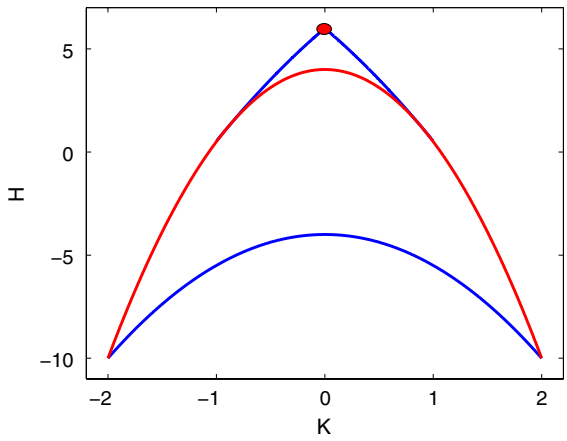

Fig. 1. Energy momentum diagram, H versus K, of the stationary system associated with Eq. (3) for identical powers of the counter-propagating beams, $S_0 = J_0 = 1$. The singular states are plotted with red and blue lines. The inside red line corresponds to a line of bitori, the points of the blue line correspond to circles, and the red point on the top of the diagram refers to a point in the original phase space (see Ref. [36] for details concerning the definitions of singular tori and singular states).

the family of singular tori. Specifically, a bitorus is topologically equivalent to two regular tori glued along a circle. Assuming $S_0 = J_0 = 1$ and using the symmetries of the energy momentum diagram, we can determine the equations of the lines that characterize the diagram depicted in Fig. 1:

$$H = 4 - \frac{7}{2}K^2, \tag{5}$$

for the singular (red) line while the boundaries (blue) lines of the diagram are defined by

$$H = 6 - K^2 \pm 2\sqrt{5}K, \tag{6}$$

and

$$H = -4 - \frac{3}{2}K^2. \tag{7}$$

The presence of a line of singularities in the energy–momentum diagram reveals the existence of the phenomenon of polarization attraction toward a continuous line of polarization states. This point is in contrast with the example of the isotropic optical fiber, whose diagram is characterized by an isolated singularity, which in turn leads to polarization attraction toward an isolated (or a discrete set of) polarization state (s) [19]. Notice that this aspect is completely analogous to the spun optical fiber considered in [22].

The fundamental problem at this point consists in characterizing the properties of the line of polarization attraction on the surface of the Poincaré sphere. The position and the shape of the line of polarization attraction depend on the polarization state of the pump injected at the fiber output, i.e., $\vec{J}(z = L)$. The analytical computation of this line proceeds as follows. Let us consider a given pump SOP, $\vec{J}(z = L)$. Using the relations $S_1^2(L) + S_2^2(L) + S_3^2(L) = 1$ and $K = S_2 + J_2$, we deduce that the energy H, defined in Eq. (4), can be expressed in terms of K and of $S_1(L)$. For instance, starting from

$$S_3(L) = \pm\sqrt{1 - S_1(L)^2 - S_2(L)^2}$$
$$S_2(L) = K - J_2(L),$$

we deduce that

$$H = -4S_1(L)J_1(L) - 8(K - J_2(L))J_2(L) \pm 4J_3(L)\sqrt{1 - S_1(L)^2 - (K - J_2(L))^2} - (K - J_2(L))^2 - J_2(L)^2. \quad (8)$$

Now, considering Eq. (5) for the singular line, we can eliminate H, which allows us to determine $S_1(L)$ as a function of K and $\vec{J}(L)$:

$$4 - \frac{7}{2}K^2 = -4S_1(L)J_1(L) - 8(K - J_2(L))J_2(L) \pm 4J_3(L)\sqrt{1 - S_1(L)^2 - (K - J_2(L))^2} - (K - J_2(L))^2 - J_2(L)^2. \quad (9)$$

Following the same procedure, one can obtain an analytical expression of $S_2(L)$ and $S_3(L)$ as a function of K and $\vec{J}(L)$, which thus defines the line of polarization attraction on the surface of the signal Poincaré sphere. This approach will be illustrated by several concrete examples in Section 4. In particular, we observe that the line of the polarization attraction is generally a closed curve, whose position and orientation depend on the pump SOP.

Before discussing the numerical simulations, let us comment on the situation in which the counter-propagating beams have different powers. In this case, the position of the singular line in the energy-momentum diagram and, thus, the corresponding position of the line of polarization attraction can only be determined numerically. The method is based on the singular reduction approach in the framework of the HB fiber, which is described briefly below (see [36] for more technical details). We introduce the following functions depending on $\vec{S}$ and $\vec{J}$:

$$\pi_1 = S_2 - J_2$$
$$\pi_2 = J_3S_3 - J_1S_1$$
$$\pi_3 = S_1J_3 + S_3J_1,$$

which satisfy the relation

$$\pi_3^2 + \pi_2^2 - \left(S_0^2 - \frac{1}{4}(K + \pi_1)^2\right)\left(J_0^2 - \frac{1}{4}(K - \pi_1)^2\right) = 0. \quad (10)$$

The Hamiltonian H can be expressed in terms of these functions:

$$H = 4\pi_2 + \frac{3}{2}\pi_1 - \frac{5}{2}K^2. \quad (11)$$

For a fixed value of K, a state is singular if the two surfaces in the (π_1, π_2, π_3)-space, defined in Eqs. (10) and (11), intersect each other with a multiplicity greater than one, e.g., if the two surfaces are tangent. We refer the reader to Ref. [34] for a complete mathematical discussion. The analysis of this general case can only be done numerically. It reveals that the line of bitori still exists for different powers S_0 and J_0. However, the length of the singular line in the energy–momentum diagram decreases as the power ratio $R = |S_0 - J_0|/J_0$ between the beams increases, and it finally disappears for $R > 2$. As we will see in Section 4.E, the numerical simulations confirm this result by showing that the phenomenon of polarization attraction disappears for $R > 2$.

4. NUMERICAL RESULTS

In this section, we illustrate the phenomenon of polarization attraction on a line of polarization states through intensive numerical simulations of the spatio-temporal Eq. (3). In all simulations, we consider 64 different initial SOPs of the signal $\vec{S}(z = 0)$, uniformly distributed over the Poincaré sphere [black dots of Fig. 2(a)] while the SOP $\vec{J}(z = L)$ of the pump is maintained fixed [green dot in Fig. 2(a)]. The input SOPs $\vec{J}(L)$ and $\vec{S}(0)$ are constant in time and the output SOPs $\vec{S}(L)$ are the constant-in-time values reached by the output signal polarizations after a transient relaxation time. We analyze different configurations characterized by specific polarization states of the pump injected at the fiber en $\vec{J}(L)$. We begin with the case where the pump and signal waves have the same power, $S_0 = J_0 = 1$. The case of different powers will be discussed later.

A. Case $\vec{J}(L) = (1/\sqrt{3}, 1/\sqrt{3}, 1/\sqrt{3})$

We start with an example of pump SOP, which is representative of the typical phenomenon of polarization attraction in a HB optical fiber. Figure 2 represents the different outputs $\vec{S}(L)$ for three different fiber lengths $L = 5$, $L = 8$, and $L = 20$, as well as the line of polarization attraction plotted from the analytic considerations discussed above, through Eq. (9). The results of the numerical simulations have been also reported in the corresponding energy–momentum diagram in Fig. 3. These results put in evidence the general behavior of the system; namely, that the efficiency of the process of polarization

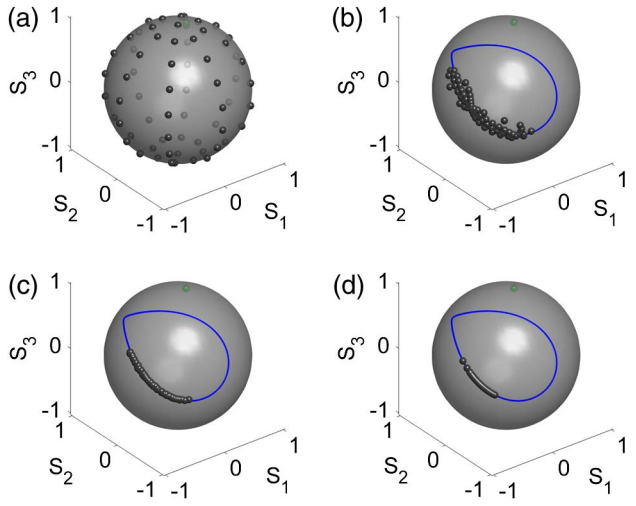

Fig. 2. Numerical simulations of the spatio-temporal Eq. (3): input (a) and output (b)–(d) signal SOPs $\vec{S}(L)$ over the Poincaré sphere for three different values of L: (b) $L = 5$, (c) $L = 8$, (d) $L = 20$. The blue line denotes the singular line of polarization attraction. The input pump $\vec{J}(L) = (1/\sqrt{3}, 1/\sqrt{3}, 1/\sqrt{3})$ is fixed (green dot). Note that the efficiency of the attraction process toward the singular line increases as the normalized fiber length L increases. Also note that the spreading of the signal SOPs on the line of polarization attraction decreases as L increases.

attraction increases with the normalized fiber length L. Indeed, the efficiency of the attraction of the signal SOPs toward the line of polarization attraction predicted by the theory (blue line) increases with the fiber length, L. At the same time, we observe that the spreading of the signal SOPs $\vec{S}(L)$ over all this line of polarization attraction decreases as the normalized length L increases. The same properties are observed for the corresponding set of points in the (H,K) energy–momentum diagram, as illustrated in Fig. 3. This corroborates the idea that there exists a direct correspondence between the singular line in the energy–momentum diagram and the line of polarization attraction on the surface of the Poincaré sphere.

The general observation that the spreading of the SOPs $\vec{S}(L)$ on the line of polarization attraction decreases as the fiber length L increases, constitutes a key property of the system. The efficiency of the attraction process can be defined in a mathematical way as follows. We introduce a measure of the distance d to the line of attraction in the energy–momentum diagram:

$$d(L) = \sqrt{\sum_i (H_i - H_s)^2}, \tag{12}$$

where the index i runs over all the initial SOPs of the signal beam. H_i and K_i are the values of the constants of the motion H and K of the corresponding stationary state and H_s is the energy of the point on the attraction line of abscissa K_i. We have performed a systematic numerical study of the attraction process for different pump SOPs $\vec{J}(z=L)$, and for different fiber lengths L, as illustrated in Fig. 4. The study reveals that the distance d rapidly tends to 0 as L increases. It is interesting to note that the value of the distance to the singular line reaches a remarkably small value for $L \simeq 10$.

The robustness of the repolarization process is also intimately related to the stability property of the stationary states on the line of polarization attraction. In fact, the stationary states on the singular line, which play the role of attractors, are only those states that are stable with respect to small spatio-temporal perturbations. The numerical simulations of Eq. (3) reveal that, by increasing L, the number of stable stationary states tends to decrease. More specifically, we observe that the stationary states on the singular line of the energy–momentum diagram become unstable above a certain threshold length L_c, which leads to the reduction of the stable part of the singular line of polarization attraction. This explains the concentration of the signal SOPs $\vec{S}(L)$ on the line of polarization attraction.

Furthermore, the simulations show that nearly half of the closed line of polarization attraction is unstable for any value of L. This is why the signal SOPs $\vec{S}(L)$ are always attracted toward the other half of the singular line, as clearly illustrated in Fig. 2. A similar feature was reported in [36], in which a general rule concerning the stability property of the stationary states was conjectured: a stationary state is stable if it exhibits a nonoscillatory evolution along the fiber coordinate z, whereas it is unstable when it exhibits an oscillatory behavior. In this respect, we remark that the problem of the stability analysis of the stationary states of this counter-propagating problem constitutes a difficult issue, which has been only addressed recently in the literature [38]. The above conjecture is remarkably well confirmed by the numerical simulations, as illustrated in Fig. 5, where the spatial dynamics of three different stationary states $\vec{S}_j$ $(j=\{a,b,c\})$ belonging to the singular line of polarization attraction are represented for increasing values of the fiber length, $L=5,8$, and 20. For the sake of clarity, only the $S_2(z)$-component is reported in Fig. 5. However, analogous results are obtained for the two other components of the Stokes vector, i.e., $S_1(z)$ and $S_3(z)$. The simulations show that the state $\vec{S}_a$ in Fig. 5 is stable for the three different values of L, a feature which is consistent with the stability conjecture, since its spatial profile does not exhibit oscillations. In opposition, the state $\vec{S}_c$ is always unstable due to its inherent oscillatory behavior. Finally, the stationary state $\vec{S}_b$ is stable for $L=5$ and $L=8$, consistently with its nonoscillatory behavior; however, it becomes oscillatory and thus unstable for $L=20$.

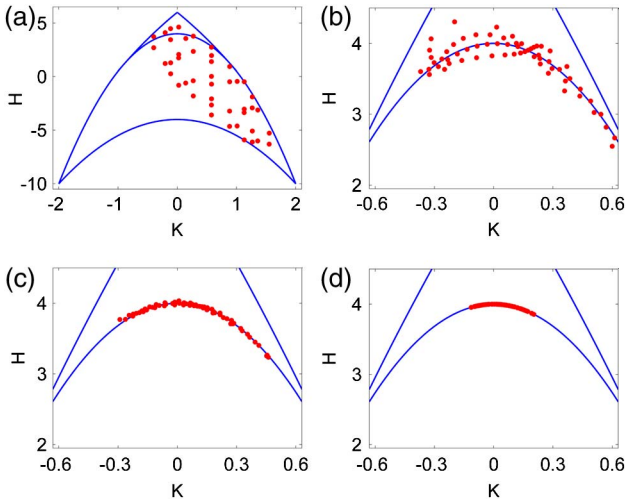

Fig. 3. Energy–momentum diagrams, H versus K, and signal SOPs corresponding to the configurations of Fig. 2. The red points represent the positions of the final SOPs in the (H,K)-diagram, the panels (a)–(d) are related to the same panels of Fig. 2. Panel (a) displays the initial condition and thus the distribution of point spreads all over the diagram. In panels (b)–(d), we observe an increasing attraction toward the parabolic line of equation $H = 4 - (7/2)K^2$. A zoom has been used in the panels (b)–(d).

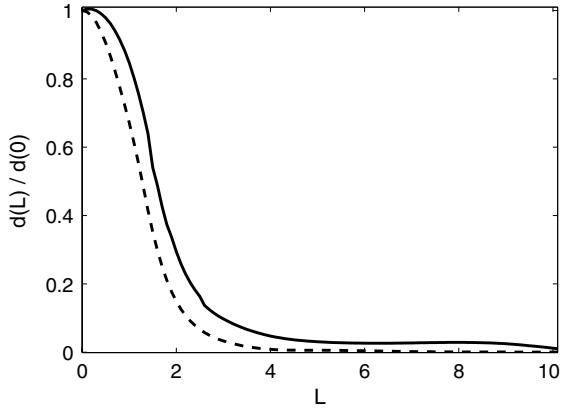

Fig. 4. Evolution of the distance d, defined in Eq. (12) as a function of the fiber length L for the input pump SOPs $\vec{J}(L) = (1/\sqrt{3}, 1/\sqrt{3}, 1/\sqrt{3})$ (solid line) and $\vec{J}(L) = (1,0,0)$ (dashed line). The distance is normalized with respect to its value for $L=0$ to improve the visualization of the convergence toward the singular line of attraction.

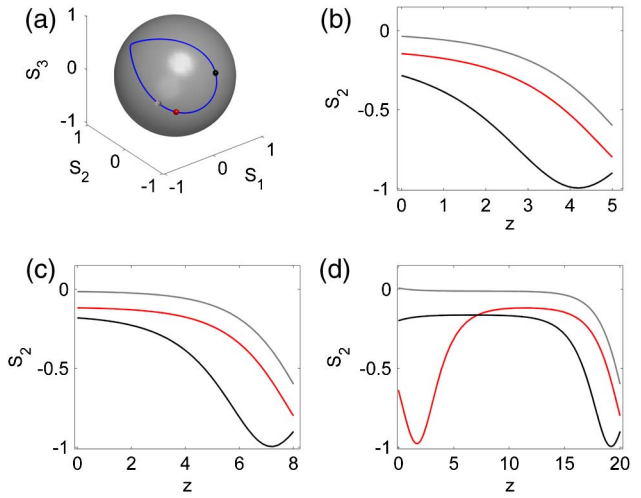

Fig. 5. (a) Three particular stationary states on the line of polarization attraction corresponding to the simulations of Figs. 1 and 2, and corresponding spatial evolutions for (b) $L = 5$, (c) $L = 8$, and (d) $L = 20$ For the sake of clarity, only the S_2-component has been reported. In panel (a): $\vec{S}_a = (-0.80, -0.58, -0.41)$ [gray dot in (a), gray lines in (b)–(d)], $\vec{S}_b = (-0.25, -0.79, -0.63)$ [red dot in (a), red lines in (b)–(d)], and $\vec{S}_c = (0.25, -0.90, 0.31)$ [black dot in (a), black lines in (b)–(d)].

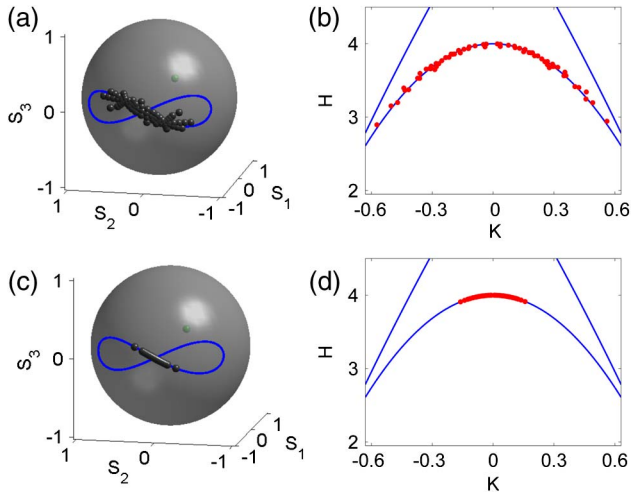

Fig. 6. Numerical simulations of the spatio-temporal Eq. (3) analogous to those reported in Figs. 2 and 3, except that the pump SOP is now $\vec{J}(L) = (1, 0, 0)$ [green dot in panels (a), (c)]. The initial condition of the signal SOPs is the same as in Fig. 2(a). (a), (b) and (c), (d) report the output signal SOPs $\vec{S}(L)$ and the corresponding positions on the energy–momentum diagram for two different normalized fiber lengths [$L = 5$ (a), (b) and $L = 20$ (c), (d)]. The blue line in panels (a), (c) represents the line of singular polarization states on the Poincaré sphere. Note that, for $L = 20$, we observe a stronger attraction toward the singular attraction line.

B. Case $\vec{J}(L) = (\pm 1, 0, 0)$

In the following, we consider particular examples of pump SOPs injected at the fiber output $\vec{J}(L)$, which lead to different interesting characteristic properties of polarization attraction. We first consider the example where the input pump is linearly polarized at $+45°$; that is, $\vec{J}(L) = (1, 0, 0)$. In this case, we deduce from Eqs. (4) and (5) that $H = -4S_1(L) - S_2(L)^2$ and $H = 4 - (7/2)S_2(L)^2$. Hence, the singular line of polarization attraction is characterized by $S_1(L) = -1 + (5/8)S_2^2(L)$. The singular line of attraction exhibits an eight-shaped figure along the S_2 axis, as illustrated in Fig. 6. The numerical simulations confirm the phenomenon of polarization attraction toward this singular line (see Fig. 6). Note that we have checked that the double loop structure of the singular line does not play any particular role in the repolarization process. As discussed above, the spreading of the signal SOPs $\vec{S}(L)$ on the line of polarization attraction is considerably reduced when the fiber length L increases. Accordingly, for very long fiber lengths, the simulations reveal the existence of a strong polarization attraction toward $S_1(L) \to -1$, i.e., a strong attraction toward the linearly polarized state at $-45°$. This is illustrated in Fig. 6(c) for $L = 20$, which shows that all initial signal SOPs are attracted very closely to the state $\vec{S}(L) = (-1, 0, 0)$. On the basis of symmetry arguments, it can be shown that an input pump linearly polarized at $-45°$ ($\vec{J}(L) = (-1, 0, 0)$) entails a polarization attraction of the signal beam to the linearly polarized state at $+45°$, a property confirmed by the numerical simulations.

C. Case $\vec{J}(L) = (0, 0, \pm 1)$

An analysis similar to that conducted above can be performed when the input pump beam is either left- or right-hand circularly polarized; that is, $\vec{J}(L) = (0, 0, \pm 1)$. In this case, we have $H = \pm 4S_3(L) - S_2(L)^2$ and $H = 4 - (7/2)S_2(L)^2$, which leads to the relation $S_3(L) = 1 - (5/8)S_2^2(L)$ for $\vec{J}(L) = (0, 0, +1)$, which is similar to that discussed above and, thus, it again leads to an eight-shaped line of attraction on the Poincaré sphere. We observe a concentration of the signal SOPs on the singular line of polarization attraction as L increases. However, because the eight-shaped line of attraction is rotated with respect to that considered in Section 4.B, here, all signal SOPs exhibit a polarization attraction toward the *same left- or right-handed circularly SOP than the pump beam*.

D. Case $\vec{J}(L) = (0, \pm 1, 0)$

We finally discuss the more complicated case in which the injected pump beam is linearly polarized along the x- (or y) axis $\vec{J}(L) = (0, \pm 1, 0)$. The singular line in the energy–momentum diagram is still characterized by Eqs. (4) and (5), which gives $K = S_2(L) \pm 1$ and $H = \mp 8S_2(L) - S_2(L)^2 - 1$. The corresponding singular line of polarization attraction on the Poincaré sphere turns out to be union of a circle of equation $S_2 = -0.6$ and the point $S_2 = +1$. We thus expect polarization attraction of the signal beam toward these specific SOPs. In particular, the output $S_2(L) = 1$ can easily be generated with the boundary conditions $\vec{S}(0) = \vec{J}(L) = (0, 1, 0)$. This stationary solution appears to be highly unstable when a small perturbation is added, so that it does not play any attractor role for the signal beam. The numerical simulations then reveal an efficient attraction of the signal SOPs toward the circle $S_2(L) = -0.6$, as expected from the theory [see Fig. 7(a)]. Note however, that, even for L sufficiently large, and with most of the output SOPs $\vec{S}(L)$ located close to the circle $S_2 = -0.6$, there exist several SOPs that are attracted toward the SOP $S_2 = -1$ [cyan dots in Fig. 7(a)]. This state of polarization is mapped to the singular line that delimits the energy–momentum diagram [cyan line in Fig. 7(b)]. We can conclude that this singular line also plays a role of attractor for the polarization dynamics. This is interesting in that the singular states on the boundaries of the energy–momentum diagram do not belong to the family of two-dimensional singular tori

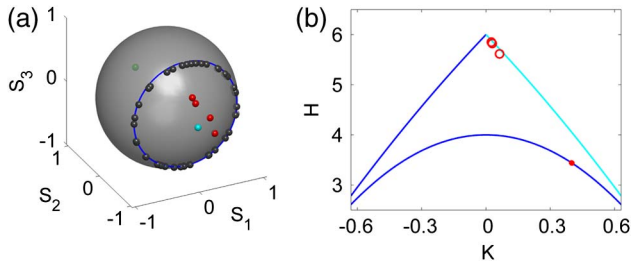

Fig. 7. Numerical simulation of the spatio-temporal Eq. (3) analogous to that reported in Figs. 2 and 3, except that the pump SOPs is now $\vec{J}(L) = (0, 1, 0)$ [green dot in (a)]. The initial condition is the same as in Fig. 2(a). The fiber length is fixed to $L = 30$. In panel (a), the singular line is a blue circle of the equation $S_2 = -0.6$. The black and red dots on the Poincaré sphere and the corresponding red dots in the energy–momentum diagram refer to the signal SOPs at the fiber output $\vec{S}(L)$. In the energy–momentum diagram, the value of K is close to 0.4. Note that some signal SOPs are attracted toward the state $S_2 = -1$ [red dots in Fig. 7(a)]. The SOP $S_2 = -1$ is associated to the singular line, which delimits the boundary of the energy–momentum diagram, represented by a cyan line in panel (b). This singular line then also plays a role of attractor for the system [see red open circles in panel (b)]. In the energy–momentum diagram, such points are characterized by $K \simeq 0$.

(see Fig. 1). This polarization effect can be interpreted as analogous with the phenomenon of self-polarization, recently identified in [29,30], in which the attraction process is due to the presence of a singular state whose topological properties do not allow to classify it as a singular torus. We finally note that, when the pump is linearly polarized along the y axis ($\vec{J}(L) = (0, -1, 0)$), basic symmetry arguments lead to a similar phenomenology: for L sufficiently large, most of the output signal SOPs $\vec{S}(L)$ are located close to $S_2 = 0.6$, the other ones being attracted by the singular line on the right boundary of the energy–momentum diagram, and are close to $S_2 = 1$ on the Poincaré sphere.

E. Case $S_0 \neq J_0$

As discussed above in Section 3, the geometrical analysis of the stationary states can be extended when the counter-propagating beams have different powers. This point is illustrated in Fig. 8. The numerical results show that the line of polarization attraction persists in the presence of unbalanced powers, though the length of the singular line in the energy–momentum diagram decreases as the power ratio $R = |S_0 - J_0|/J_0$ increases, and finally disappears for $R > 2$. This means that, if $R > 2$, then the system no longer exhibits (nontrivial) stationary solutions associated to singular states in the energy–momentum diagram. Accordingly, the phenomenon of polarization attraction is expected to disappear when $R > 2$, a property confirmed by the numerical simulations of the spatio-temporal Eq. (3). This provides supplementary evidence that the phenomenon of polarization attraction seems to be inherently associated to the existence of singular stationary states in the system.

The numerical simulations also show that the efficiency of the process of polarization attraction tends to decrease as the ratio R in power increases. More specifically, the simulations reveal a novel dynamical feature of the system for unbalanced powers: some input signal SOPs $\vec{S}(0)$ no longer relax to a stationary stable state as discussed above for $S_0 = J_0$, but instead lead to an output signal $\vec{S}(t, L)$ that exhibits complex temporal dynamics that can be either periodic, quasi-periodic, or chaotic. Note, in this respect, that the counter-propagating four-wave interaction is known to exhibit a rich spatio-temporal dynamics, as discussed in pioneering works, e.g., [39–41]. Intensive numerical simulations of Eq. 3 have proved that the occurrence of the nonstationary dynamics is related to the relative position between $\vec{S}(0)$ and $\vec{J}(L)$ over the Poincaré sphere, as well as to the power ratio R and the fiber length L. For a fixed ratio R and length L, any SOPs $\vec{S}(0)$ evolves toward a stationary state if R or L are sufficiently small. Note also that nonstationary dynamics can appear for $R = 0$ if $L \gg 20$.

The numerical results reported in Fig. 8 provide a clear physical picture of the system dynamics described above. They show that there exists a competition between the attraction process, which tends to align the signal SOPs $\vec{S}(L)$ along the singular line of polarization attraction (black dots in Fig. 8), and the nonstationary dynamics, which tend to spread the signal SOPs all over the sphere (gray dots in Fig. 8). In this example, the powers are taken to be $S_0 = 1.5$, $J_0 = 1.0$ ($R = 0.5$), the pump SOP $\vec{J}(L) = (1, 0, 0)$, and the fiber lengths have been fixed to $L = 5$ and $L = 20$. The signal SOPs are represented for the specific time $t = 900$.

As already discussed, for $R \neq 0$, the position of the singular line of polarization attraction cannot be determined analytically, but only numerically. The study reveals that this singular line depends on the power ratio R, as illustrated in Fig. 8. Here again, the numerical simulations confirm the theoretical predictions and reveal a strong attraction toward the singular line in the energy–momentum diagram. This attraction increases for larger values of L. For $R > 0$, there exists some intermediate values of the fiber length (of the order of $L \simeq 10$), for which a compromise can be found between the two

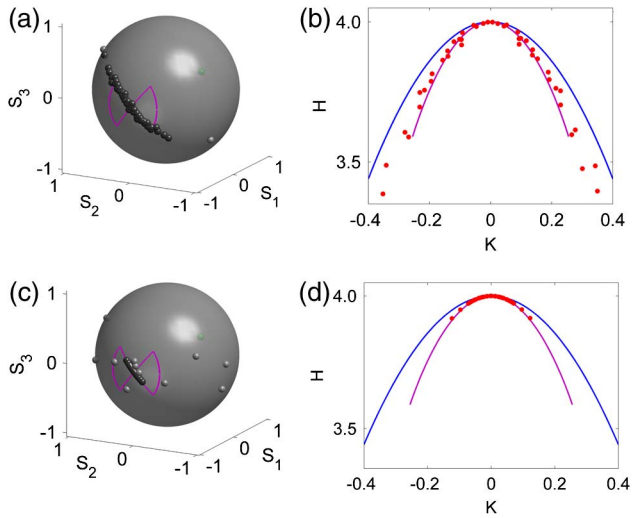

Fig. 8. Numerical simulation of the spatio-temporal Eq. (3) analogous to that reported in Figs. 2 and 3, except that now the pump SOPs $\vec{J}(L) = (1, 0, 0)$ and the powers are $S_0 = 1.5$, $J_0 = 1.0$. The initial condition is the same as in Fig. 2(a). Two different fiber lengths have been considered: $L = 5$ (a), (b) and $L = 20$ (c), (d). The pink lines in (a) and (c) denote the singular line of polarization attraction. The blue and the pink lines in the energy–momentum diagrams (b), (d) represent the lines of singular states for the cases $S_0 = J_0 = 1$ and $S_0 = 1.5, J_0 = 1.0$, respectively. The black points in panels (a), (c) depict signal SOPs associated with a stationary dynamics while gray points are associated to nonstationary dynamics (plotted at time $t = 900$). In the energy–momentum diagrams (b) and (d), only the stationary states have been plotted.

competing mechanisms; namely, the attraction toward the singular line and the nonstationary dynamics, which tend to spread the signal SOPs all over the Poincaré sphere.

5. CONCLUSION

We have shown that the phenomenon of polarization attraction in a highly birefringent fiber with counter-propagating beams is characterized by a polarization of the signal SOPs toward a specific singular line on the surface of the Poincaré sphere. A detailed description of this attraction process has been given through the geometrical analysis of the singularities of the corresponding stationary system. Although the existence of a singular line of polarization attraction was already identified in the example of spun fibers [22,36], the properties of the corresponding process were not analyzed in detail in previous works. A numerical study of the stability of the stationary solutions reveals a key property of the attraction process: the spreading of signal SOPs on the line of polarization attraction decreases in a substantial way as the normalized fiber length increases. This property entails the existence of novel forms of polarization attraction whose properties depend on the injected pump SOP. More precisely, we have shown that, (i) a pump linearly polarized at $\pm 45°$ along the principal axes of the fiber entails a signal polarization to a linearly polarized state at $\mp 45°$, (ii) a linearly polarized pump entails a signal attraction toward a specific circle on the Poincaré sphere, and (iii) a right- or left-hand circularly polarized pump plays the role of an attractor for the unpolarized forward signal. Moreover, we have seen that the singular line that delimits the energy–momentum diagram can also play the role of attractor for a linearly polarized injected pump.

A systematic study of the system has also been performed for different powers of the counter-propagating beams. It reveals that the attraction process persists in the presence of unbalanced powers, although its efficiency is shown to decrease in a substantial way. We conclude by remarking that the presence of relatively small propagation losses, in the range ~0.2–0.4 dB/km, decreases the powers of the beams without affecting the polarization process.

Besides the characterization of the phenomenon of polarization attraction, the theory discussed here can also be extended to study the stability properties of soliton solutions in a medium of finite extension [31,42]. Work is in progress to extend these preliminary works to more general soliton systems, such as gap solitons and three-wave interaction solitons.

ACKNOWLEDGMENTS

We acknowledge the financial support of the European Research Council under the Grant Agreement 306633 PETAL ERC project, the CNRS, the Labex ACTION program (Contract ANR-11-LABX-01-01) and the Conseil Régional de Bourgogne under the PHOTCOM program.

REFERENCES

1. J. E. Heebner, R. S. Bennink, R. W. Boyd, and R. A. Fisher, "Conversion of unpolarized light to polarized light with greater than 50% efficiency by photorefractive two-beam coupling," Opt. Lett. **25**, 257–259 (2000).
2. S. Pitois, A. Picozzi, G. Millot, H. R. Jauslin, and M. Haelterman, "Polarization and modal attactors in conservative counterpropagating four-wave interaction," Europhys. Lett. **70**, 88 (2005), doi:10.1209/epl/i2004-10469-9.
3. B. Crosignani, B. Daino, and P. Di Porto, "Depolarization of light due to the optical Kerr effect in low-birefringence single-mode fibers," J. Opt. Soc. Am. B **3**, 1120–1123 (1986).
4. A. Picozzi, "Entropy and degree of polarization for nonlinear optical waves," Opt. Lett. **29**, 1653–1655 (2004).
5. H. Prakash and D. Singh, "Change in coherence properties and degree of polarization of light propagating in a lossless isotropic nonlinear Kerr medium," J. Phys. B **41**, 045401 (2008).
6. M. Martinelli, M. Cirigliano, M. Ferrario, L. Marazzi, and P. Martelli, "Evidence of Raman-induced polarization pulling," Opt. Express **17**, 947–955 (2009).
7. S. Sergeyev, S. Popov, and A. T. Friberg, "Virtually isotropic transmission media with fiber Raman amplifier," IEEE J. Quantum Electron. **46**, 1492–1497 (2010).
8. L. Ursini, M. Santagiustina, and L. Palmieri, "Raman nonlinear polarization pulling in the pump depleted regime in randomly birefringent fibers," IEEE Photon. Technol. Lett. **23**, 254–256 (2011).
9. S. V. Sergeyev, "Activated polarization pulling and decorrelation of signal and pump states of polarization in a fiber Raman amplifier," Opt. Express **19**, 24268–24279 (2011).
10. V. Kozlov, J. Nuno, J. D. Ania-Castanon, and S. Wabnitz, "Theoretical study of optical fiber Raman polarizers with counterpropagating beams," J. Lightwave Technol. **29**, 341–347 (2011).
11. N. J. Muga, M. F. S. Ferreira, and A. N. Pinto, "Broadband polarization pulling using Raman amplification," Opt. Express **19**, 18707–18712 (2011).
12. S. Sergeyev, "Fiber Raman amplification in a two-scale spun fiber," Opt. Mater. Express **2**, 1683–1689 (2012).
13. S. Sergeyev and S. Popov, "Two-section fiber optic Raman polarizer," IEEE J. Quantum Electron. **48**, 56–60 (2012).
14. P. Morin, S. Pitois, and J. Fatome, "Simultaneous polarization attraction and Raman amplification of a light beam in optical fibers," J. Opt. Soc. Am. B **29**, 2046–2052 (2012).
15. Z. Shmilovitch, N. Primerov, A. Zadok, A. Eyal, S. Chin, L. Thevenaz, and M. Tur, "Dual-pump push-pull polarization control using stimulated Brillouin scattering," Opt. Express **19**, 25873–25880 (2011).
16. M. I. Dykman, B. Golding, L. I. McCann, V. N. Smelyanskiy, D. G. Luchinsky, R. Mannella, and P. V. E. McClintock, "Activated escape of periodically driven systems," Chaos **11**, 587–594 (2001).
17. D. Sugny, A. Picozzi, S. Lagrange, and H. R. Jauslin, "Role of singular tori in the dynamics of spatiotemporal nonlinear wave systems," Phys. Rev. Lett. **103**, 034102 (2009).
18. S. Lagrange, D. Sugny, A. Picozzi, and H. R. Jauslin, "Singular tori as attractors of four-wave interaction systems," Phys. Rev. E **81**, 016202 (2010).
19. E. Assémat, S. Lagrange, A. Picozzi, H. R. Jauslin, and D. Sugny, "Complete nonlinear polarization control in an optical fiber system," Opt. Lett. **35**, 2025–2027 (2010).
20. V. V. Kozlov and S. Wabnitz, "Theoretical study of polarization attraction in high-birefringence and spun fibers," Opt. Lett. **35**, 3949–3951 (2010).
21. V. V. Kozlov, J. Nuno, and S. Wabnitz, "Theory of lossless polarization attraction in telecommunication fibers," J. Opt. Soc. Am. B **28**, 100–108 (2011).
22. E. Assémat, D. Dargent, A. Picozzi, H. R. Jauslin, and D. Sugny, "Polarization control in spun and telecommunication optical fibers," Opt. Lett. **36**, 4038–4040 (2011).
23. M. Guasoni, V. V. Kozlov, and S. Wabnitz, "Theory of polarization attraction in parametric amplifiers based on telecommunication fibers," J. Opt. Soc. Am. B **29**, 2710–2720 (2012).
24. M. Guasoni and S. Wabnitz, "Nonlinear polarizers based on four-wave mixing in high-birefringence optical fibers," J. Opt. Soc. Am. B **29**, 1511–1520 (2012).
25. S. Pitois, J. Fatome, and G. Millot, "Polarization attraction using counter-propagating waves in optical fiber at telecommunication wavelengths," Opt. Express **16**, 6646–6651 (2008).
26. P. Morin, J. Fatome, C. Finot, S. Pitois, R. Claveau, and G. Millot, "All-optical nonlinear processing of both polarization state and intensity profile for 40 Gbit/s regeneration applications," Opt. Express **19**, 17158–17166 (2011).

27. V. V. Kozlov, J. Fatome, P. Morin, S. Pitois, G. Millot, and S. Wabnitz, "Nonlinear repolarization dynamics in optical fibers: transient polarization attraction," J. Opt. Soc. Am. B **28**, 1782–1791 (2011).
28. B. Stiller, P. Morin, D. M. Nguyen, J. Fatome, S. Pitois, E. Lantz, H. Maillotte, C. R. Menyuk, and T. Sylvestre, "Demonstration of polarization pulling using a fiber-optic parametric amplifier," Opt. Express **20**, 27248–27253 (2012).
29. J. Fatome, S. Pitois, P. Morin, D. Sugny, E. Assémat, A. Picozzi, H. R. Jauslin, G. Millot, V. V. Kozlov, and S. Wabnitz, "A universal optical all-fiber omnipolarizer," Sci. Rep. **2**, 938–946 (2012).
30. P.-Y. Bony, M. Guasoni, E. Assémat, S. Pitois, D. Sugny, A. Picozzi, H. R. Jauslin, and J. Fatome, "Optical flip-flop memory and data packet switching operation based on polarization bistability in a telecommunication optical fiber," J. Opt. Soc. Am. B **30**, 2318–2325 (2013).
31. V. V. Kozlov and S. Wabnitz, "Instability of optical solitons in the boundary value problem for a medium of finite extension," Lett. Math. Phys. **96**, 405–413 (2011).
32. V. V. Kozlov, K. Turitsyn, and S. Wabnitz, "Nonlinear repolarization in optical fibers: polarization attraction with copropagating beams," Opt. Lett. **36**, 4050–4052 (2011).
33. V. V. Kozlov, M. Barozzi, A. Vannucci, and S. Wabnitz, "Lossless polarization attraction of co-propagating beams in telecom fibers," J. Opt. Soc. Am. B **30**, 530–540 (2013).
34. R. H. Cushman and L. M. Bates, *Global Aspects of Classical Integrable Systems* (Birkhauser, 1997).
35. K. Efstathiou and D. A. Sadovskii, "Normalization and global analysis of perturbations of the hydrogen atom," Rev. Mod. Phys. **82**, 2099–2154 (2010).
36. E. Assémat, A. Picozzi, H. R. Jauslin, and D. Sugny, "Hamiltonian tools for the analysis of optical polarization control," J. Opt. Soc. Am. B **29**, 559–571 (2012).
37. V. I. Arnold, *Mathematical Methods of Classical Mechanics* (Springer-Verlag, 1989).
38. K. S. Turitsyn and S. Wabnitz, "Stability analysis of polarization attraction in optical fibers," Opt. Commun. **307**, 62–66 (2013).
39. S. Trillo and S. Wabnitz, "Intermittent spatial chaos in the polarization of counterpropagating beams in a birefringent optical fiber," Phys. Rev. A **36**, 3881–3884 (1987).
40. A. L. Gaeta, R. W. Boyd, J. R. Ackerhalt, and P. W. Milonni, "Instabilities and chaos in the polarizations of counterpropagating light fields," Phys. Rev. Lett. **58**, 2432–2435 (1987).
41. D. David, D. D. Holm, and M. V. Tratnik, "Hamiltonian chaos in nonlinear optical polarization dynamics," Phys. Rep. **187**, 281–367 (1990).
42. E. Assémat, A. Picozzi, H. R. Jauslin, and D. Sugny, "Instabilities of optical solitons and Hamiltonian singular solutions in a medium of finite extension," Phys. Rev. A **84**, 013809 (2011).